




# Solvothermal Synthesis of PtNi Nanoparticle Thin Film Cathode with Superior Thermal Stability for Low Temperature Solid Oxide Fuel Cells

Jiyeon Shin<sup>1</sup> · Kittiwat Kamlungsua<sup>2</sup> · Hao-Yang Li<sup>1</sup> · Pei-Chen Su<sup>1,2</sup> 

Received: 18 July 2023 / Revised: 13 October 2023 / Accepted: 18 October 2023 / Published online: 10 February 2024  
© The Author(s), under exclusive licence to Korean Society for Precision Engineering 2024

## Abstract

This work adopts solvothermal synthesis to fabricate PtNi nanoparticles as thin film cathodes with superior resistance against thermally driven agglomeration for low temperature solid oxide fuel cells (LT-SOFCs) operating at 450 °C. Metal-based porous electrodes are common choices for thin film LT-SOFCs, but pure metals with high density nanoscale porosities are vulnerable to thermal agglomeration, which imposes challenges to maintaining high performance with long-term stability. Typical Pt-based thin film cathodes are previously reported to sustain a record high 600 °C of thermal annealing with acceptable morphological stability, but the temperature is still too low for practical LT-SOFC application. In this work, the solvothermal synthesized PtNi nanoparticle thin films show superior thermal stability, sustaining 10 h of annealing at 800 °C without significant agglomeration observed. By controlling the length of synthesis time, the particle sizes and Pt loading ratio can be varied. The cost-effective solvothermal synthesis process for the fabrication of PtNi thin film cathode is a promising way for LT-SOFC manufacturing in scale as it involves no vacuum process like typical sputtering.

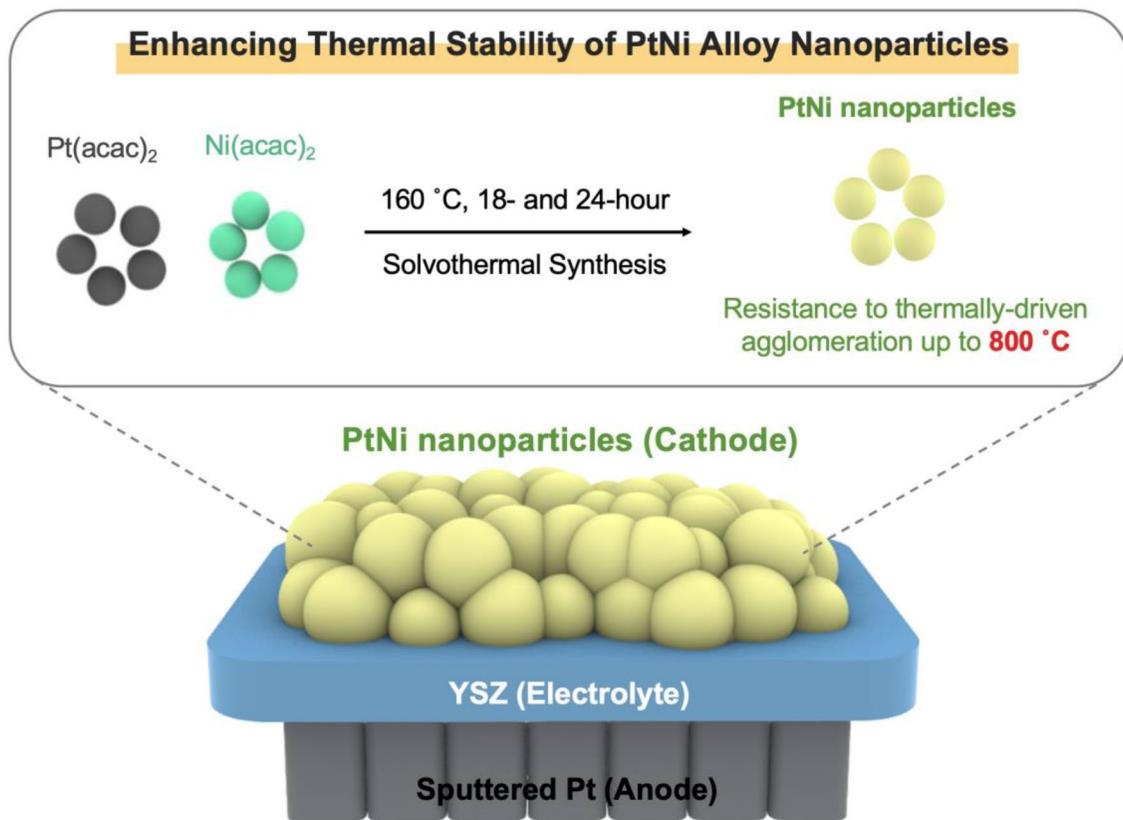
---

✉ Pei-Chen Su  
peichensu@ntu.edu.sg

<sup>1</sup> School of Mechanical and Aerospace Engineering,  
Nanyang Technological University, 50 Nanyang Avenue,  
Singapore 639798, Singapore

<sup>2</sup> Energy Research Institute @ NTU (ERI@N),  
Interdisciplinary Graduate School, Nanyang Technological  
University, 50 Nanyang Drive, Singapore 637553, Singapore

## Graphical Abstract



**Keywords** Solvothermal synthesis · PtNi nanoparticles · Low temperature solid oxide fuel cells · Thin film cathode · Thermal stability · Agglomeration

## 1 Introduction

Low temperature solid oxide fuel cells (LT-SOFCs) operating at temperatures below 600 °C are promising in resolving chronic issues that exist in conventional high temperature SOFCs (HT-SOFCs) running at 800–1000 °C [1–5]. The research focus for LT-SOFCs has been on developing high performance cathode materials to tackle the sluggish oxygen reduction reactions (ORR) at the greatly decreased cell operating temperature. Conventional HT-SOFCs adopt oxide materials, especially mixed ionic electronic conducting (MIEC) perovskites such as  $\text{La}_{0.6}\text{Sr}_{0.4}\text{Co}_{0.2}\text{Fe}_{0.8}\text{O}_{3-8}$  [6, 7],  $\text{PrBa}_{0.5}\text{Sr}_{0.5}\text{Co}_{1.5}\text{Fe}_{0.5}\text{O}_{5+8}$  [8, 9], or  $\text{Sr}_2\text{Fe}_{1.5}\text{Mo}_{0.5}\text{O}_{6-8}$  [10, 11], as cathodes to achieve high performance with good thermal stability. However, MIEC electrodes require higher temperatures to fully activate the cathode catalytic activities, and the LT-SOFC temperature below 550 °C is too low to utilize these materials.

On the other hand, unlike HT-SOFCs, which require the use of refractory oxides with sintering to form porous

electrodes due to the high operating temperature, LT-SOFCs allow a wider range of electrode material selection even pure metals. Catalytically active metals such as Ni, Pt, Ag, and their alloys or their composites with oxides are the major choices [12–21]. Reported studies have shown that porous metals or porous metal-oxide composites with good catalytic activity at below 600 °C temperature range are more feasible cathodes for LT-SOFCs [12, 22]. The major issue of utilizing metal at elevated temperatures is the long-term thermal stability of the porous metal components. Metal cathode layers for LT-SOFCs are usually fabricated using DC magnetron sputtering or RF sputtering at high base pressure to obtain a porous electrode morphology [12–16]. These as-sputtered porous electrodes have a high density of nanoporous surface area of electrochemically active sites but are also vulnerable to thermally driven agglomerations at elevated temperatures due to the high surface energy. Therefore, maintaining the thermal stability of the high density of porosity in the metal cathode is of great interest.

Strategies to maintain a high electrode porosity of LT-SOFCs for stable performance include applying a thin oxide capping layer over the sputtered porous electrode [14], improving the adhesion between sputtered porous metal electrode and electrolyte substrate [16], and alloying Pt with another catalytically active metal such as Ni [15] (Fig. S1). These three strategies combined were reported to effectively preserve the nanoporous features of the sputtered porous electrode at up to 600 °C. In particular, the alloying strategy, which preserves the body of the entire sputtered electrode layer, is most effective compared to only preserving the surface and interfacial porosities. The alloying of Pt with other metallic elements M (M = Au, Co, Cu, Fe, and Ni) was also reported to enhance the ORR activity of Pt-based catalysts and to reduce Pt loading which makes Pt-M alloy even more attractive in the application of LT-SOFCs.

Among the reported Pt-M alloys, the PtNi combination shows the highest ORR activity close to pure Pt in the volcano plot, as well as better resistance to agglomeration than pure Pt [23, 24] up to 600 °C [13, 15]. However, this temperature is only slightly higher than the targeted 450 °C operating temperature of LT-SOFCs, and significant degradation was still observed in our previously reported PtNi work (26% after 48 h) [15]. Also, the composition uniformity of sputtered PtNi over the entire electrode surface area is questionable, which can worsen the electrode degradation driven by electrical current.

Therefore, the preparation of thermally stable PtNi nanoparticle electrodes with good composition uniformity to replace the thermally vulnerable sputtered PtNi is important for stable LT-SOFC performance. This work demonstrated the solvothermal synthesis process for such PtNi nanoparticles with good thermal stability and composition uniformity. Solvothermal synthesis of catalyst nanoparticles was only reported for low temperature applications [25–27], but no demonstration was found for high temperature applications. We synthesized PtNi nanoparticles with control of particle cluster size and composition by varying the synthesis time. The morphological stability of the nanoparticles sustained annealing at temperature up to 800 °C without significant agglomeration, which surpassed our previous reported record at up to 600 °C.

## 2 Experimental Section

### 2.1 Solvothermal Synthesis of PtNi Nanoparticles

Figure 1 illustrates the solvothermal synthesis of PtNi nanoparticles. Pt(acac)<sub>2</sub> and Ni(acac)<sub>2</sub> were used as metal precursors to form the PtNi alloy nanoparticles. We employed a combination of two chemical agents: polyvinylpyrrolidone (PVP)

and hexadecyltrimethylammonium bromide (CTAB) as surfactants. PVP serves as an effective agent for preventing the PtNi nanoparticles from agglomeration by creating a protective barrier between them during the solvothermal process [28, 29]. CTAB acts as a surfactant, as well as promotes the formation of larger nanoparticle sizes [30]. A stoichiometric amount of 0.098 g platinum (II) acetylacetonate (Pt(acac)<sub>2</sub>, 97%, Sigma Aldrich), 0.064 g nickel (II) acetylacetonate (Ni(acac)<sub>2</sub>, 95%, Sigma Aldrich), 0.687 g polyvinylpyrrolidone (PVP, average molecular weight ~55,000, Sigma Aldrich), and 50 mM hexadecyltrimethylammonium bromide (CTAB, 99%, Sigma Aldrich) (Fig. 1a) were dissolved in 50 ml of N, N-dimethylformamide (DMF, 99.8%, Sigma Aldrich) under magnetic stirring at 50 °C until the mixture reached a clear green color, as illustrated in Fig. 1b. The resulting green color solution was transferred into a Teflon-lined stainless-steel autoclave, as shown in Fig. 1c. Subsequently, the tightly sealed autoclave was covered by sands to ensure uniform thermal environments and put into a furnace maintained at 160 °C for 6-, 12-, 18-, and 24-h (Fig. 1d). The solution containing nanoparticles (Fig. 1e) was rinsed in ethanol with centrifugation three times to separate the PtNi precipitate, as shown in Fig. 1f. The collected black PtNi precipitates were used for future studies (Fig. 1g).

### 2.2 Characterizations of PtNi Nanoparticles Crystallinity, Size, and Composition

The crystalline structure of the as-prepared PtNi nanoparticles was characterized by X-ray diffraction (D8 Advance, Cu-K, Bruker) between 20° and 90° of 2θ angle. The morphology of the nanoparticles and the structure of the cell were observed by field-emission scanning electron microscopy (FESEM, JSM-7600F, JEOL). Detailed observation of nanoparticle size was carried out by high-resolution transmission electron microscopy (HR-TEM, JEM-2100F, JEOL) at 200 kV equipped with EDX. The composition of the PtNi was quantified by inductively coupled plasma optical emission spectroscopy (ICP-OES, Optima™ 8300, PerkinElmer®). The particle size distribution was analyzed by using Image J software.

### 2.3 Thermal Stability Test of PtNi Nanoparticles by High Temperature Annealing

The dispersed PtNi nanoparticles were drop-casted and vacuum-dried on Si chips to form thin film electrodes, followed by thermal annealing at a tube furnace at 450, 600, and 800 °C in ambient air for 10 h. The morphological evolutions with an annealing time of 10 h and temperatures at 450 °C, 600 °C, and 800 °C were observed by FESEM (JSM-7600F, JEOL). The thermal stability of pure Pt nanoparticles prepared by the same process was also observed for comparison.

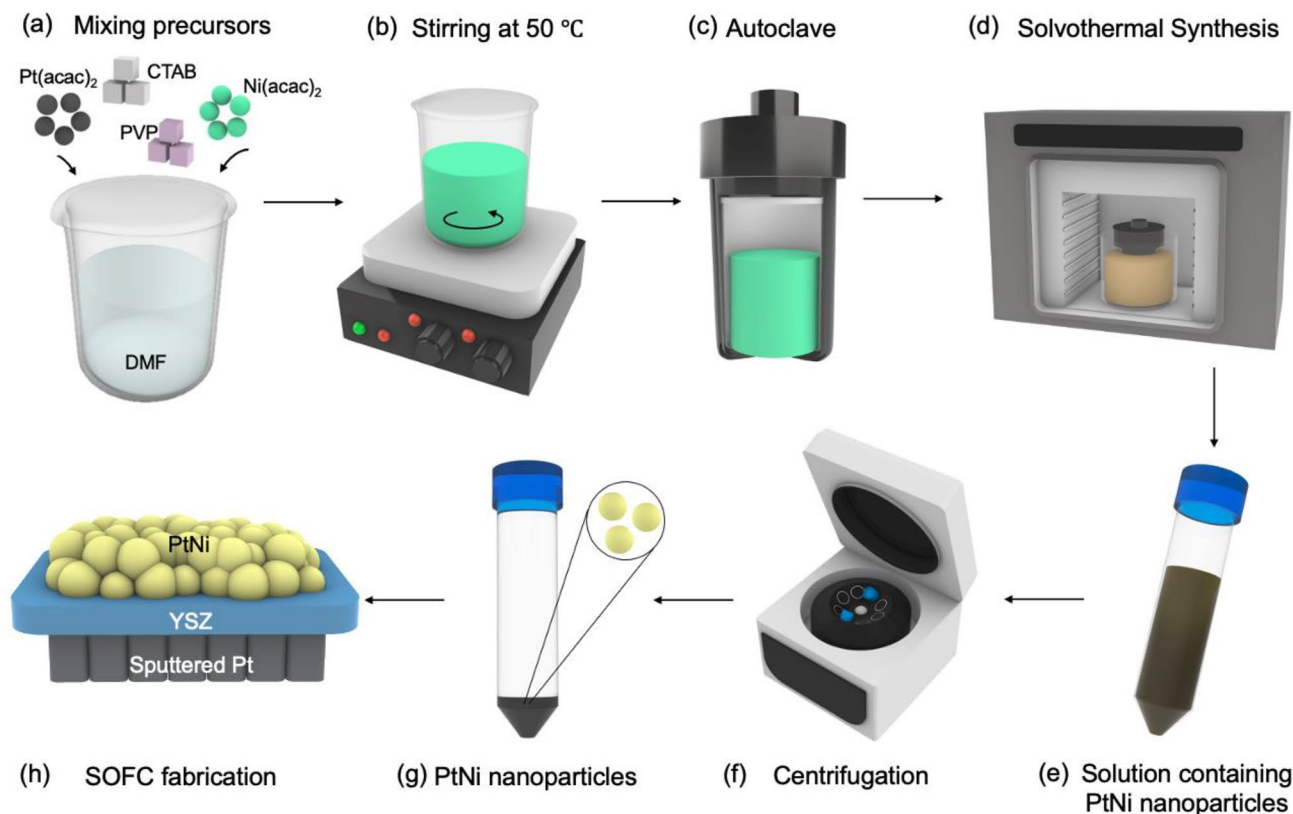


**Fig. 1** Solvothermal synthesis of PtNi nanoparticles. **a** Mixing metal precursors; **b** stirring at 50 °C; **c** transferring into an autoclave; **d** annealing; **e** solution containing as-synthesized PtNi nanoparticles; **f** centrifugation; **g** PtNi precipitate; **h** SOFC fabrication

The long-term stability of 10, 20, 30, 40, and up to 50 h of annealing was done to the 18-h synthesized PtNi nanoparticles at 450 °C to verify if any further morphological changes of PtNi nanoparticle with time.

## 2.4 SOFCs Test Using PtNi Cathodes

A half-cell SOFC (schematic in Fig. 1h) was prepared for the polarization resistance test. To form the cathode thin film, PtNi nanoparticles were drop-casted onto one side of a single-crystalline (100) YSZ electrolyte substrate (10 × 10 × 0.2 mm, Latech Scientific Supply Pte. Ltd., Singapore), followed by an intermittent baking process at 200 °C for 1 h. The anode thin film with 100 nm thickness was deposited using DC magnetron sputtering on the other side of the YSZ substrate.

The fuel cell using PtNi alloy cathode was tested by draining the current for an I-V curve at 450 °C using linear sweep voltammetry (LSV) with an electrochemical potentiostat (SP-200, BioLogic®). The anode was fed with pure hydrogen gas at a flow rate of 20 sccm, and the cathode was exposed to ambient air.

## 3 Results and Discussion

### 3.1 PtNi Nanoparticle Size, Composition, and Crystallinity vs. Solvothermal Time

The particle morphology evolution with increasing solvothermal time of 6-, 12-, 18-, and 24-h was first characterized with TEM. As shown in Fig. 2a, the nanoparticles formed larger aggregated clusters about 30 to 40 nm, and the aggregated cluster size increases as solvothermal time increases and saturates at 18-h. Figure 2b shows the individual cluster of nanoparticles with an individual nanoparticle contour highlighted in white dashed lines for all solvothermal times. The individual particle sizes were around 5 to 10 nm and also showed an increasing trend with solvothermal time. The interplanar spacing around 0.221 nm and 0.131 nm correspond to the (111) and (220) planes of PtNi alloys (Fig. 2c), respectively [31–33], which confirms the particles synthesized were indeed PtNi alloys.

The particle size distribution (Fig. 2d and Fig. S2, along with a summary in Table. S1.) shows a consistent increase in the size of the aggregated particle



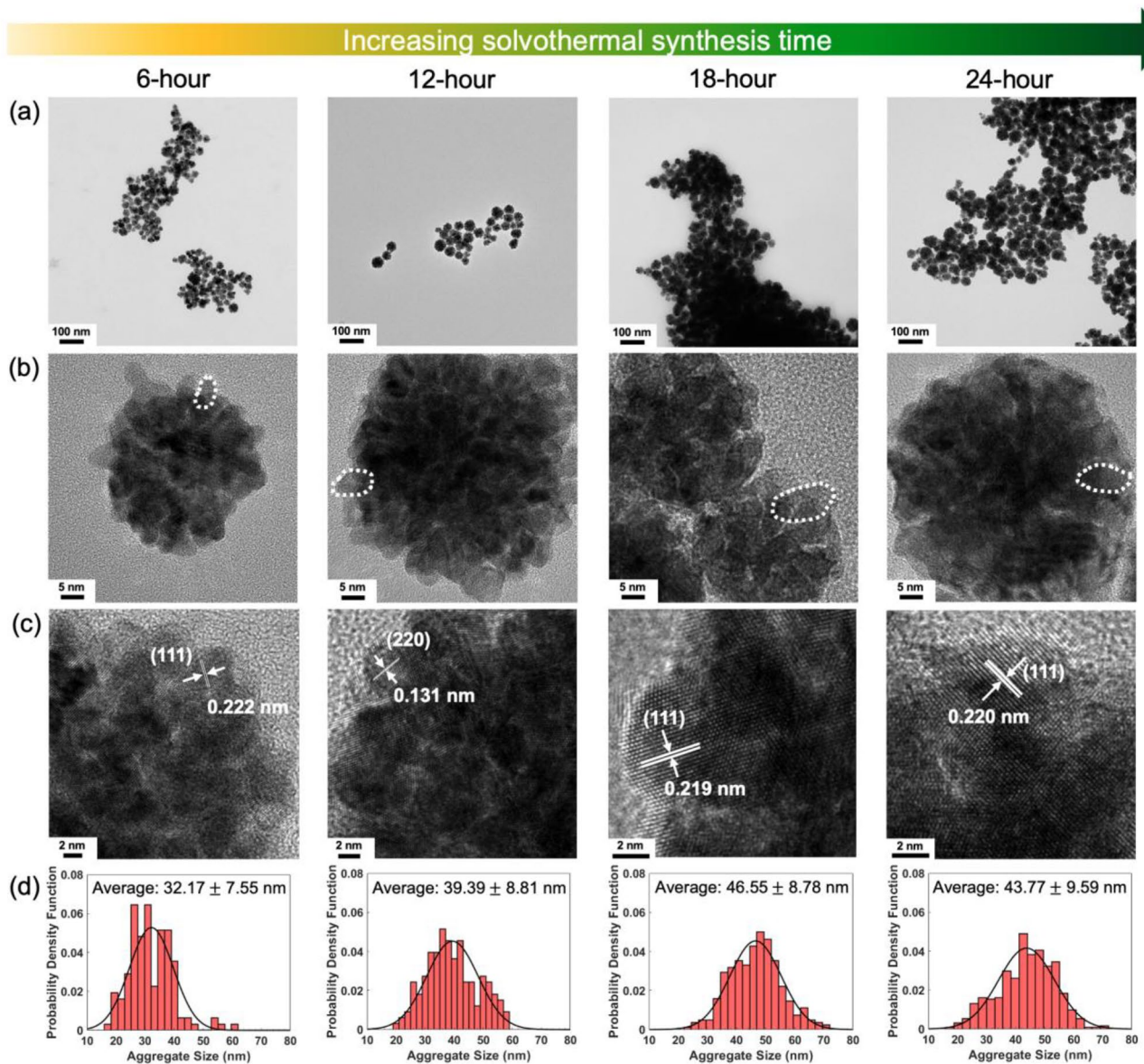


**Fig. 2** **a** TEM images showing PtNi nanoparticle forming aggregated clusters. **b** Bright-field TEM images identifying individual particles within a particle cluster. **c** HRTEM images with measurement of

inter-planar spacing, showing the PtNi alloy formation. **d** The distribution of aggregate cluster size distribution for PtNi nanoparticles with different solvothermal times at 160 °C

clusters with increasing solvothermal time up to 18-h (6-h:  $32.17 \text{ nm} \pm 7.55 \text{ nm}$ , 12-h:  $39.39 \text{ nm} \pm 8.81 \text{ nm}$ , 18-h:  $46.55 \text{ nm} \pm 8.78 \text{ nm}$ ). For the 24-h particles, no significant further growth from 18-h was observed ( $43.77 \text{ nm} \pm 9.59 \text{ nm}$ ). This can be explained by LaMer's mechanism [34–37] that for prolonged synthesis time, the diffusion of  $\text{Pt}^{+2}$  and  $\text{Ni}^{+2}$  ions to the nucleation site can be slower. Similar trend of individual particle size increase was also observed from the TEM image in Fig. 2b, where the particle size peaks at 18-h without a significant increase at 24-h. Considering the cost-effectiveness of

fabrication time, the shorter 18-h time was selected for PtNi nanoparticle synthesis.

The composition of the synthesized PtNi particles also evolves with solvothermal time. As illustrated in Fig. 3a, the atomic percentage of Pt decreases with increasing solvothermal time, from 50.04% (6-h) to 37.53% (24-h). In addition, the Ni and Pt distribution was uniform throughout the alloy (Fig. 3b, also see Fig. S3 for details of elemental distribution under different solvothermal times). The synthesized PtNi particles were confirmed to have intermetallic phases for all solvothermal synthesis times. Figure 3c shows the FCC

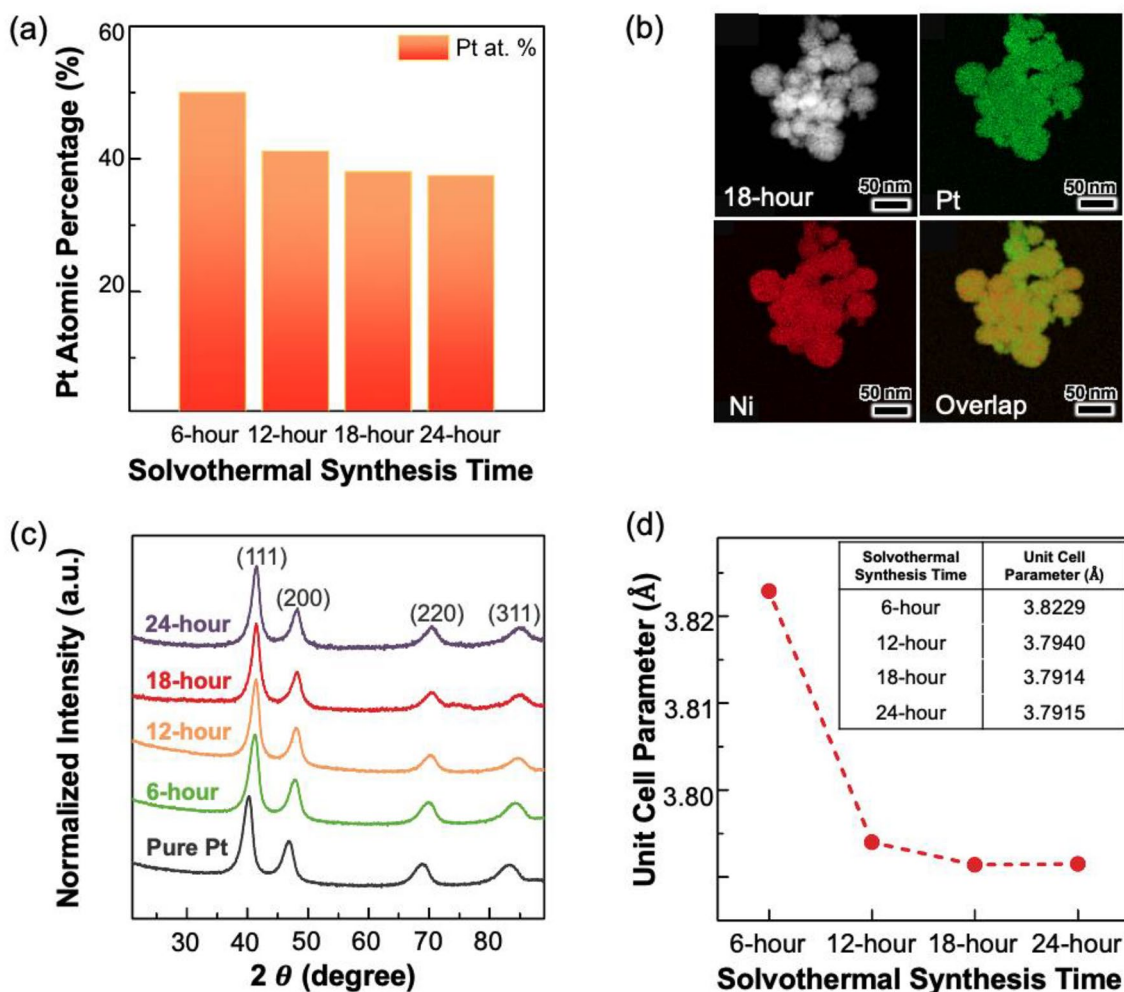


**Fig. 3** **a** Composition of PtNi nanoparticles synthesized at 160 °C for different solvothermal times. **b** HAADF-STEM image and elemental mapping of the PtNi nanoparticles synthesized at 160 °C for 18-h of solvothermal time (green: Pt; red: Ni; scale bar: 50 nm). **c** XRD patterns of the as-prepared PtNi nanoparticles with various solvothermal

times (6-, 12-, 18-, and 24-h) at 160 °C and **d** unit cell parameters derived from Rietveld refinement and corresponding parameters for the PtNi nanoparticles prepared at various solvothermal times, presented in the table

structure with peak positions corresponding to (111), (200), (220), and (311) planes. The peak positions of PtNi particles are consistent with that of pure Pt nanoparticles [38–40], except that a 2-degree shift of the peaks toward the higher angles was observed as the solvothermal time increased. The peak positions corresponded to around 41°, 48°, 71°, and 85°, which are in between pure Pt and pure Ni peaks [15, 38, 41], meaning the synthesized powders are intermediate PtNi alloy nanoparticles. The unit cell lengths of all as-synthesized powders (extracted by Rietveld refinement, Fig. 3d, also see Table. S2 for details) were in between pure Pt (3.923 Å) and pure Ni (3.523 Å) [23, 42], where longer solvothermal process rendered smaller unit cell length (from 3.8229 Å for 6-h to 3.7915 Å for 24-h), likely due to the pure Ni having smaller unit cell length that penetrated Pt crystals when forming PtNi alloy nanoparticles [40].

### 3.2 Thermal Stability of PtNi Nanoparticles

The synthesized nanoparticles were purposefully annealed at very high temperatures up to 800 °C to confirm their superior thermal stability. The FESEM images of pure Pt, and PtNi nanoparticles showing the morphology changes with increasing temperature are summarized in Fig. 4. Pure Pt showed very weak resistance even at the lowest annealing temperature of 450 °C. For PtNi alloys synthesized at all solvothermal times, the morphology did not change significantly at 450 and 600 °C. Only at the highest annealing temperature of 800 °C did the 6- and 12-h synthesized PtNi show more obvious agglomeration. The 18- and 24-h synthesized PtNi were obviously more resistant to thermal agglomeration at 800 °C than 6- and 12-h. The better resistivity of 18- and 24-h synthesized

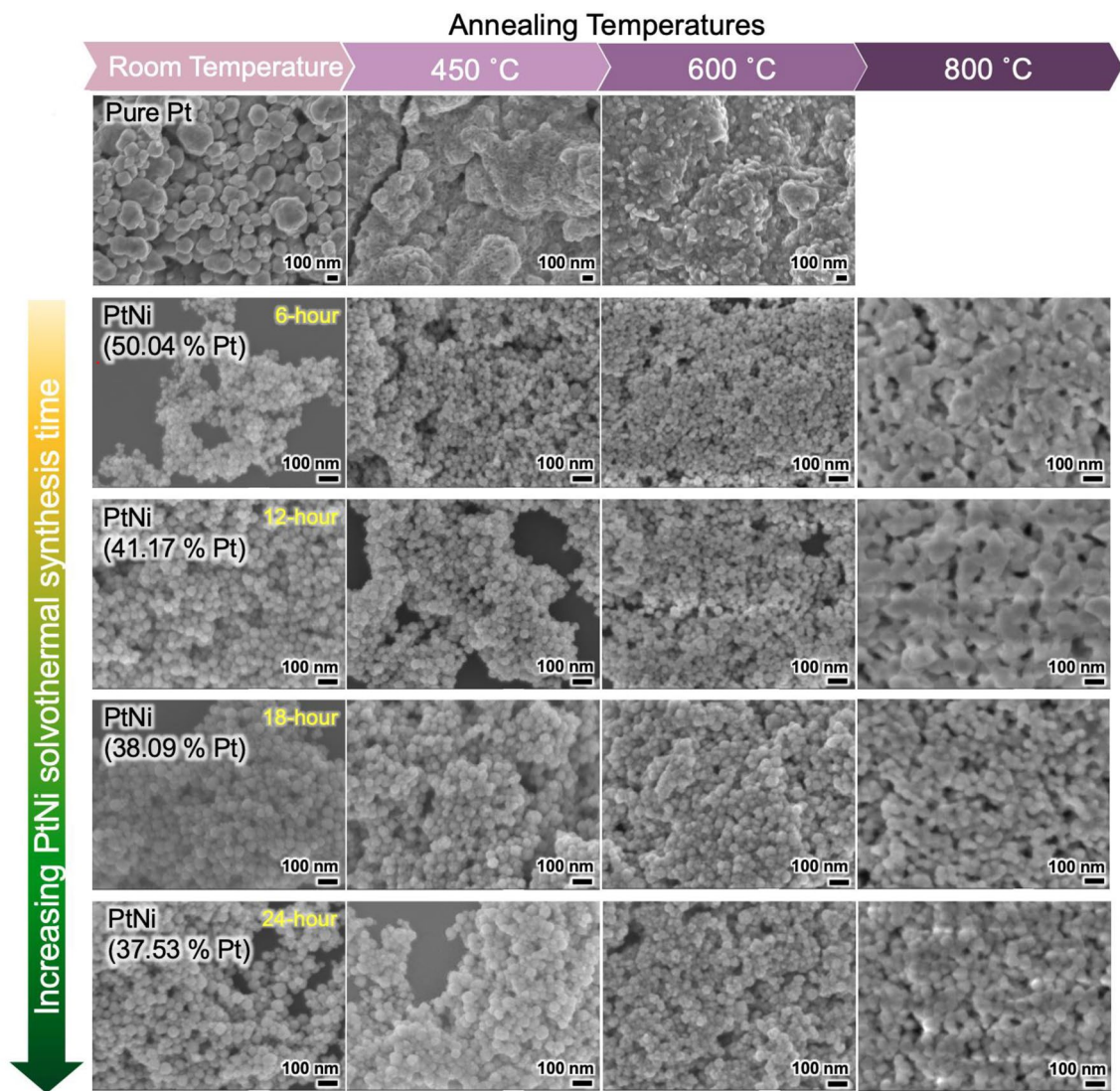


**Fig. 4** FESEM images of pure Pt and the as-prepared PtNi nanoparticles thin film cathodes prepared at different solvothermal times (6-, 12-, 18-, and 24-h) and annealed in ambient air for 10 h at 450, 600, and 800 °C

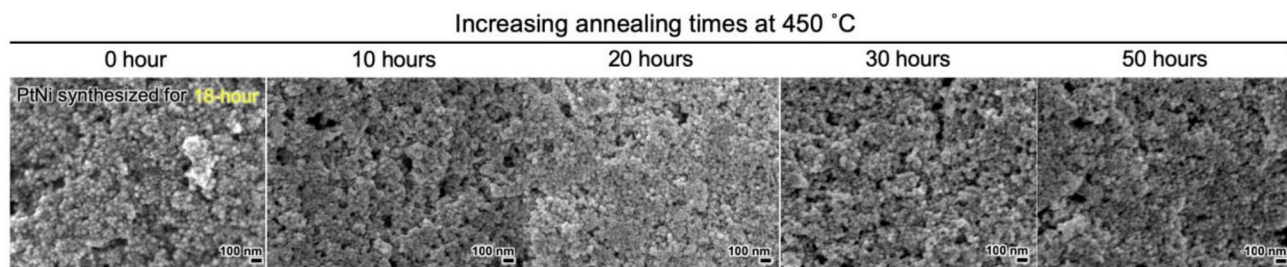
PtNi alloys can be due to their larger particle size that gives lower surface energy as well as the higher Ni contents that affect the melting point. The 18-h PtNi particles were eventually selected for making cathode in our later fuel cell test in a half-cell for its excellent thermal stability and shorter synthesis time than the 24-h particles.

We further examined the morphological stability of the 18-h nanoparticles by longer annealing time in the air at 450 °C, which is the target operating temperature for LT-SOFCs. As expected, no noticeable morphology change was observed from 0 up to 50 h of annealing time (Fig. 5).

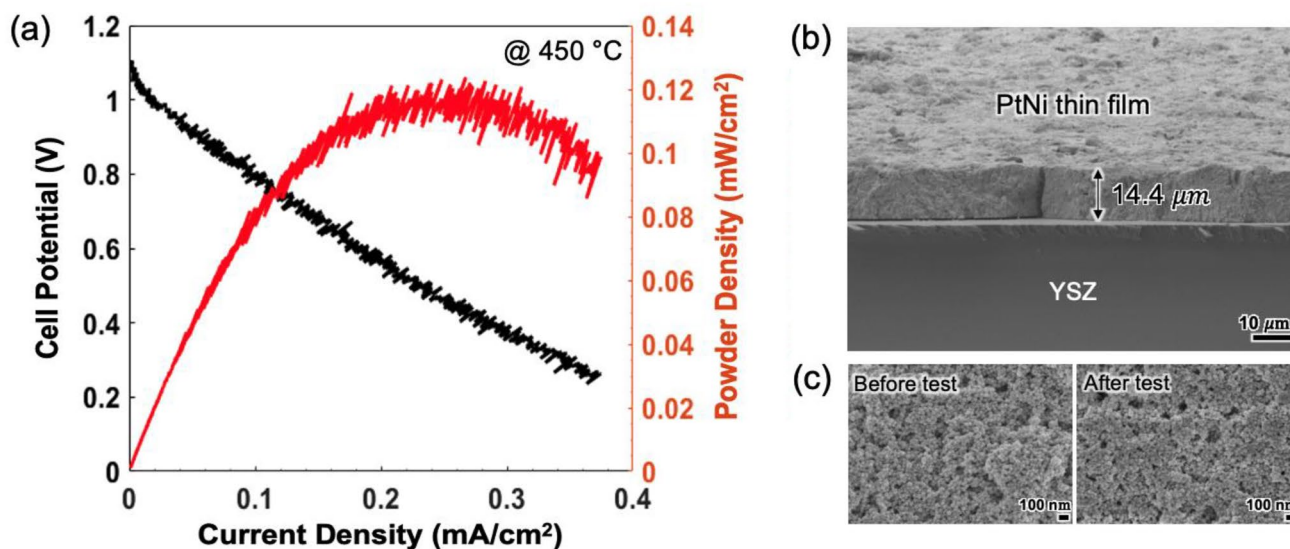
### 3.3 Fuel Cell Test Using 18-h PtNi Nanoparticle Cathode

Figure 6b shows the morphology of the PtNi thin film cathode drop-casted on a YSZ substrate with a thickness of 14.4  $\mu\text{m}$ . Fuel cell performance of the PtNi/YSZ/Pt LT-SOFC at 450 °C in the polarization curve (Fig. 6a) shows a maximum power density of 0.124  $\text{mW}/\text{cm}^2$  using a 200  $\mu\text{m}$  thickness of YSZ substrate and porous sputtered Pt anode. Due to the extensive effort to obtain good adhesion of the drop-casted electrode in our lab, electrochemical impedance





**Fig. 5** FESEM images of the PtNi nanoparticles solvothermal synthesized at 160 °C for 18-h annealing at 450 °C in ambient air for 0, 10, 20, 30, and 50 h. No noticeable morphology change was observed



**Fig. 6** **a** Polarization curve of the fuel cell with the solvothermal synthesized PtNi nanoparticle cathode running at 450 °C with air at the cathode and pure H<sub>2</sub> at the anode. **b** Cross-sectional view of the PtNi

nanoparticle cathode with a thickness of 14.4 μm. **c** PtNi nanoparticle cathode before and after fuel cell test showing minimum morphology change

measurements to further understand the performance of PtNi electrodes are still underway. Also, the cell performance was limited due to the high ohmic resistance of YSZ, but it can be greatly improved when using a thin film micro-SOFC with a sub-micrometer thickness electrolyte. It is noteworthy that with current flowing through during the fuel cell test at 450 °C, there was still no noticeable morphological changes were observed (Fig. 6c).

It is hard to deny that in the “nanoparticle level”, the 5 to 10 nm particles were likely already agglomerating during the annealing at 450, 600, and 800 °C and during the cell test at 450 °C. In our FESEM image observations shown in Figs. 4, 5, and 6, what we observed was the “cluster level” of thermal stability which showed no significant changes. Nevertheless, the impressive resistance to 800 °C of annealing at cluster level has justified the superior thermal stability of PtNi thin film cathodes fabricated by solvothermal synthesis. More detailed characterization in the “nanoparticle level”

including morphology changes using TEM and electrochemical performance stability using electrochemical impedance spectroscopy is underway.

## 4 Conclusions

PtNi alloy nanoparticles with superior thermal stability were synthesized via solvothermal methods. Control over nanoparticle size and alloying composition was achieved by varying the solvothermal synthesis times. The synthesized PtNi nanoparticle thin film showed excellent resistance to thermally driven agglomeration at 800 °C by maintaining the porous morphology. Fuel cells using PtNi nanoparticle drop-casted as a thin film cathode showed a decent maximum power density of 0.124 mW/cm<sup>2</sup> at a low temperature of 450 °C and can be largely improved if a thinner electrolyte can be used. The solvothermal synthesis process is



simple and cost-effective for the fabrication of thermally stable PtNi nanoparticles. This approach provides a promising alternative to expensive vacuum-based deposition techniques, ensuring uniform distribution of PtNi nanoparticles for SOFC electrodes with exceptional thermal stability. We believe this approach can shed light on the production and practical applications of PtNi nanoparticles for SOFC cathodes with exceptional thermal stability.

**Supplementary Information** The online version contains supplementary material available at <https://doi.org/10.1007/s40684-023-00576-7>.

**Acknowledgements** The authors thank the financial support from the Singapore Ministry of Education under AcRF Tier 1 Project No. RG73/22.

**Author Contributions** JS: Conceptualization, Investigation, Writing-Original draft preparation, Writing-Review and Editing. KK: Conceptualization, Methodology, Investigation. H-YL: Investigation. P-CS: Supervision, Writing-Review & Editing.

## Declarations

**Conflict of Interest** The authors declare that they have no known competing financial interests or personal relationships that could have appeared to influence the work reported in this paper. The authors declare the following financial interests/personal relationships which may be considered as potential competing interests:

## References

- Zhang, J., Ricote, S., Hendriksen, P. V., & Chen, Y. (2022). Advanced materials for thin-film solid oxide fuel cells: Recent progress and challenges in boosting the device performance at low temperatures. *Advanced Functional Materials*, *32*, 2111205.
- Baldi, F., Moret, S., Tammi, K., & Maréchal, F. (2020). The role of solid oxide fuel cells in future ship energy systems. *Energy*, *194*, 116811.
- Jo, M., Kim, S., & Lee, C. (2022). Morphology engineering for compact electrolyte layer of solid oxide fuel cell with roll-to-roll eco-production. *International Journal of Precision Engineering and Manufacturing-Green Technology*, *9*, 431–441.
- Ji, S., & Kim, W. (2022). Is coating oxide on porous metal thin-film for low-temperature solid oxide fuel cell cathode a panacea for performance enhancement? *International Journal of Precision Engineering and Manufacturing*, *23*, 445–451.
- Ji, S., Kim, Y., & Cha, S. W. (2022). Operating cost savings in the atomic layer deposition process of ultrathin electrolyte for solid oxide fuel cells by applying oxygen plasma. *International Journal of Precision Engineering and Manufacturing*, *23*, 573–579.
- Chen, Y., Choi, Y., Yoo, S., Ding, Y., Yan, R., Pei, K., et al. (2018). A highly efficient multi-phase catalyst dramatically enhances the rate of oxygen reduction. *Joule*, *2*, 938–949.
- Choi, H. J., Bae, K., Grieshammer, S., Han, G. D., Park, S. W., Kim, J. W., et al. (2018). Surface tuning of solid oxide fuel cell cathode by atomic layer deposition. *Advanced Energy Materials*, *8*, 1802506.
- Choi, S., Kucharczyk, C. J., Liang, Y., Zhang, X., Takeuchi, I., Ji, H.-I., et al. (2018). Exceptional power density and stability at intermediate temperatures in protonic ceramic fuel cells. *Nature Energy*, *3*, 202–210.
- Tian, Y., Li, J., Liu, Y., Yang, J., Liu, B., Jia, L., et al. (2018). Preparation and properties of  $\text{PrBa}_{0.5}\text{Sr}_{0.5}\text{Co}_{1.5}\text{Fe}_{0.5}\text{O}_{5+\delta}$  as novel oxygen electrode for reversible solid oxide electrochemical cell. *International Journal of Hydrogen Energy*, *43*, 12603–12609.
- Li, H.-Y., & Su, P.-C. (2023). Applied current on the suppression of strontium segregation in  $\text{Sr}_2\text{Fe}_{1.5}\text{Mo}_{0.5}\text{O}_6-\delta$  electrode for improved oxygen evolution reaction. *Applied Materials Today*, *31*, 101769.
- Muñoz-García, A. B., Bugaris, D. E., Pavone, M., Hodges, J. P., Huq, A., Chen, F., et al. (2012). Unveiling structure–property relationships in  $\text{Sr}_2\text{Fe}_{1.5}\text{Mo}_{0.5}\text{O}_6-\delta$ , an electrode material for symmetric solid oxide fuel cells. *Journal of the American Chemical Society*, *134*, 6826–6833.
- Huang, H., Nakamura, M., Su, P., Fasching, R., Saito, Y., & Prinz, F. B. (2006). High-performance ultrathin solid oxide fuel cells for low-temperature operation. *Journal of the Electrochemical Society*, *154*, B20.
- Wang, X., Huang, H., Holme, T., Tian, X., & Prinz, F. B. (2008). Thermal stabilities of nanoporous metallic electrodes at elevated temperatures. *Journal of Power Sources*, *175*, 75–81.
- Liu, K.-Y., Fan, L., Yu, C.-C., & Su, P.-C. (2015). Thermal stability and performance enhancement of nano-porous platinum cathode in solid oxide fuel cells by nanoscale ZrO<sub>2</sub> capping. *Electrochemistry Communications*, *56*, 65–69.
- Liu, K.-Y., Yoon, Y. J., Lee, S. H., & Su, P.-C. (2017). Sputtered nanoporous PtNi thin film cathodes with improved thermal stability for low temperature solid oxide fuel cells. *Electrochimica Acta*, *247*, 558–563.
- Liu, K.-Y., Baek, J. D., Ng, C. S., & Su, P.-C. (2018). Improving thermal stability of nanoporous platinum cathode at platinum/yttria-stabilized zirconia interface by oxygen plasma treatment. *Journal of Power Sources*, *396*, 73–79.
- Van Herle, J., & McEvoy, A. (1994). Oxygen diffusion through silver cathodes for solid oxide fuel cells. *Journal of Physics and Chemistry of Solids*, *55*, 339–347.
- Yu, C.-C., Baek, J. D., Su, C.-H., Fan, L., Wei, J., Liao, Y.-C., et al. (2016). Inkjet-printed porous silver thin film as a cathode for a low-temperature solid oxide fuel cell. *ACS Applied Materials & Interfaces*, *8*, 10343–10349.
- Kamlungua, K., Lee, T.-H., Lee, S., Su, P.-C., & Yoon, Y.-J. (2021). Inkjet-printed Ag@SDC core-shell nanoparticles as a high-performance cathode for low-temperature solid oxide fuel cells. *International Journal of Hydrogen Energy*, *46*, 30853–30860.
- Ji, S., Kim, W., Han, S., Jeong, S., & Park, T. (2023). Stability enhancement of reformate-fueled, low-temperature solid oxide fuel cell with nickel thin-film anode by water bubbling. *International Journal of Precision Engineering and Manufacturing-Green Technology*, *10*, 999–1006.
- Shin, J. W., Lee, S., Go, D., Yang, B. C., Kim, T., Jo, S. E., et al. (2023). Nanometer Yttria-doped ceria shell by atomic layer deposition over porous Pt for improved oxygen reduction reactions. *International Journal of Precision Engineering and Manufacturing-Green Technology*, *10*, 773–781.
- Tucker, M. C. (2010). Progress in metal-supported solid oxide fuel cells: A review. *Journal of Power Sources*, *195*, 4570–4582.
- Stephens, I. E., Bondarenko, A. S., Grønbjerg, U., Rossmeisl, J., & Chorkendorff, I. (2012). Understanding the electrocatalysis of oxygen reduction on platinum and its alloys. *Energy and Environmental Science*, *5*, 6744–6762.
- Greeley, J., Stephens, I., Bondarenko, A., Johansson, T. P., Hansen, H. A., Jaramillo, T., et al. (2009). Alloys of platinum and early transition metals as oxygen reduction electrocatalysts. *Nature Chemistry*, *1*, 552–556.
- Du, J.-J., Chen, C., Gan, Y.-L., Zhang, R.-H., Yang, C.-Y., & Zhou, X.-W. (2014). Facile one-pot hydrothermal synthesis of Pt nanoparticles and their electrocatalytic performance. *International Journal of Hydrogen Energy*, *39*, 17634–17637.

26. Wang, Y., Cai, F., Guo, P., Lei, Y., Xi, Q., & Wang, F. (2019). Short-time hydrothermal synthesis of CuBi<sub>2</sub>O<sub>4</sub> nanocolumn arrays for efficient visible-light photocatalysis. *Nanomaterials*, *9*, 1257.
27. Yang, Z., Wang, M., Liu, G., Chen, M., Ye, F., Zhang, W., et al. (2020). Octahedral Pt-Ni nanoparticles prepared by pulse-like hydrothermal method for oxygen reduction reaction. *Ionics*, *26*, 293–300.
28. Koczur, K. M., Mourdikoudis, S., Polavarapu, L., & Skrabalak, S. E. (2015). Polyvinylpyrrolidone (PVP) in nanoparticle synthesis. *Dalton Transactions*, *44*, 17883–17905.
29. Yin, J., Wang, J., Li, M., Jin, C., & Zhang, T. (2012). Iodine ions mediated formation of monomorphic single-crystalline platinum nanoflowers. *Chemistry of Materials*, *24*, 2645–2654.
30. Vadivel, M., Babu, R. R., Ramamurthi, K., & Arivanandhan, M. (2016). CTAB cationic surfactant assisted synthesis of CoFe<sub>2</sub>O<sub>4</sub> magnetic nanoparticles. *Ceramics International*, *42*, 19320–19328.
31. Yang, P., Yuan, X., Hu, H., Liu, Y., Zheng, H., Yang, D., et al. (2018). Solvothermal synthesis of alloyed PtNi colloidal nanocrystal clusters (CNCs) with enhanced catalytic activity for methanol oxidation. *Advanced Functional Materials*, *28*, 1704774.
32. Wang, M., Chen, X., Xu, W., Wang, Z., He, P., & Lu, Z. (2022). Gram-scale synthesis of carbon-supported Sub-5 nm PtNi nanocrystals for efficient oxygen reduction. *Metals*, *12*, 1078.
33. Leteba, G. M., Wang, Y.-C., Slater, T. J., Cai, R., Byrne, C., Race, C. P., et al. (2021). Oleylamine aging of PtNi nanoparticles giving enhanced functionality for the oxygen reduction reaction. *Nano Letters*, *21*, 3989–3996.
34. Wang, F., Richards, V. N., Shields, S. P., & Buhro, W. E. (2014). Kinetics and mechanisms of aggregative nanocrystal growth. *Chemistry of Materials*, *26*, 5–21.
35. Schladt, T. D., Schneider, K., Schild, H., & Tremel, W. (2011). Synthesis and bio-functionalization of magnetic nanoparticles for medical diagnosis and treatment. *Dalton Transactions*, *40*, 6315–6343.
36. Vreeland, E. C., Watt, J., Schober, G. B., Hance, B. G., Austin, M. J., Price, A. D., et al. (2015). Enhanced nanoparticle size control by extending LaMer's mechanism. *Chemistry of Materials*, *27*, 6059–6066.
37. Kirakosyan, A., Kim, J., Lee, S. W., Swathi, I., Yoon, S.-G., & Choi, J. (2017). Optical properties of colloidal CH<sub>3</sub>NH<sub>3</sub>PbBr<sub>3</sub> nanocrystals by controlled growth of lateral dimension. *Crystal Growth and Design*, *17*, 794–799.
38. Li, W., Sun, Z., Tian, D., Nevirkovets, I. P., & Dou, S.-X. (2014). Platinum dendritic nanoparticles with magnetic behavior. *Journal of Applied Physics*, *116*, 033911.
39. Liu, Y., Chen, H., Tian, C., Geng, D., Wang, D., & Bai, S. (2019). One-pot synthesis of highly efficient carbon-supported polyhedral Pt<sub>3</sub>Ni alloy nanoparticles for oxygen reduction reaction. *Electrocatalysis*, *10*, 613–620.
40. Chen, S., Wu, H., Tao, J., Xin, H., Zhu, Y., & Chen, J. (2019). Pt–Ni seed-core-frame hierarchical nanostructures and their conversion to nanoframes for enhanced methanol electro-oxidation. *Catalysts*, *9*, 39.
41. Wang, H., Kou, X., Zhang, J., & Li, J. (2008). Large scale synthesis and characterization of Ni nanoparticles by solution reduction method. *Bulletin of Materials Science*, *31*, 97–100.
42. Strasser, P., Koh, S., Anniyev, T., Greeley, J., More, K., Yu, C., et al. (2010). Lattice-strain control of the activity in dealloyed core-shell fuel cell catalysts. *Nature Chemistry*, *2*, 454–460.

**Publisher's Note** Springer Nature remains neutral with regard to jurisdictional claims in published maps and institutional affiliations.

Springer Nature or its licensor (e.g. a society or other partner) holds exclusive rights to this article under a publishing agreement with the author(s) or other rightsholder(s); author self-archiving of the accepted manuscript version of this article is solely governed by the terms of such publishing agreement and applicable law.



**Jiyoona Shin** is currently pursuing her Ph.D. degree in the School of Mechanical and Aerospace Engineering at Nanyang Technological University, Singapore. Her research interests focus on noble metal nanocatalysts, metal-oxide interfaces, and surface coating and modification of energy conversion devices, specifically solid oxide cells.



**Kittiwat Kamlungsua** received his Ph.D. degree in the Interdisciplinary Graduate School at Nanyang Technological University, Singapore, in 2022. His research thesis focused on the development of cathodes for solid oxide cells. Currently, he works for Enserv Power Co., Ltd. in Thailand as an R&D consultant, he is in charge of the project 'Asymmetric Supercapacitor', aiming at using layered oxide materials as its cathode.



**Hao-Yang Li** is currently pursuing his Ph.D. degree in the School of Mechanical and Aerospace Engineering at Nanyang Technological University, Singapore. His research interests focus on functional ceramic material and energy conversion devices, specifically solid oxide cells.



**Professor Pei-Chen Su** is an associate professor in the School of Mechanical and Aerospace Engineering and Cluster Director of the Energy Research Institute at Nanyang Technological University, Singapore. She is also the vice president of the Thin Films Society. Her research focuses on the surface coating and modification of energy conversion devices, high-temperature nanoionics, and solid-state ionics at the device level, specifically solid oxide cells. Currently, she concerns about multiscale additive manufacturing for 3D/4D printing or polymer and composites.